LANGMUIR

pubs.acs.org/Langmuir Article

# Colloid Interaction Energies for Surfaces with Steric Effects and Incompressible and/or Compressible Roughness

Scott A. Bradford,* Salini Sasidharan, Hyunjung Kim, Allan Gomez-Flores, Tiantian Li, and Chongyang Shen

Cite This: *Langmuir* 2021, 37, 1501−1510 Read Online

ACCESS | Metrics & More | Article Recommendations | Supporting Information

**ABSTRACT:** Colloid aggregation and retention in the presence of macromolecular coatings (e.g., adsorbed polymers, surfactants, proteins, biological exudates, and humic materials) have previously been correlated with electric double layer interactions or repulsive steric interactions, but the underlying causes are not fully resolved. An interaction energy model that accounts for double layer, van der Waals, Born, and steric interactions as well as nanoscale roughness and charge heterogeneity on both surfaces was extended, and theoretical calculations were conducted to address this gap in knowledge. Macromolecular coatings may produce steric interactions in the model, but non-uniform or incomplete surface coverage may also create compressible nanoscale roughness with a charge that is different from the underlying surface. Model results reveal that compressible nanoscale roughness reduces the energy barrier height and the magnitude of the primary minimum at separation distances exterior to the adsorbed organic layer. The depth of the primary minimum initially alters (e.g., increases or decreases) at separation distances smaller than the adsorbed organic coating because of a decrease in the compressible roughness height and an increase in the roughness fraction. However, further decreases in the separation distance create strong steric repulsion that dominates the interaction energy profile and limits the colloid approach distance. Consequently, adsorbed organic coatings on colloids can create shallow primary minimum interactions adjacent to organic coatings that can explain enhanced stability and limited amounts of aggregation and retention that have commonly been observed. The approach outlined in this manuscript provides an improved tool that can be used to design adsorbed organic coatings for specific colloid applications or interpret experimental observations.

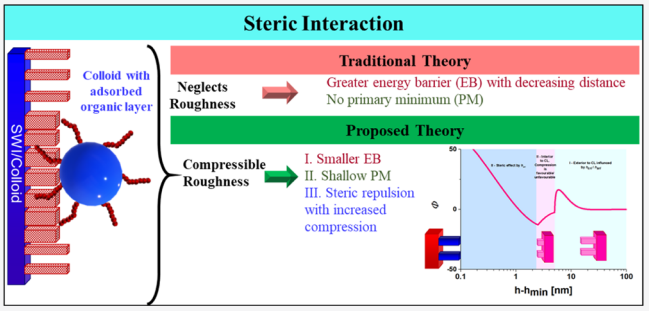


## INTRODUCTION

Knowledge of processes that influence colloid transport and fate, including microorganisms and nanoparticles (NPs), is needed for many industrial and environmental applications.[1,2] However, many colloid suspensions are found to aggregate and/or be retained on surfaces rapidly.[3] This limits colloid mobility and hampers their utility in specific processes.[4] To overcome this limitation, colloid suspensions are frequently designed to minimize aggregation and retention.[5]

Interaction energy calculations are commonly used to predict conditions that are favorable or unfavorable for colloid aggregation and/or retention.[3−5] Typically, van der Waals and electrostatic double-layer interactions for spherical particles are considered in these calculations, but they may be extended to include other particle shapes,[6,7] particle orientations,[7,8] and forces.[3,4,9] The ability of colloids to interact with a surface depends on the depths of the primary and secondary minima, and the height of the energy barrier. When the secondary minimum is insignificant (e.g., for NPs), a colloid's ability to interact in a primary minimum depends on the height of the energy barrier. It is not possible for a colloid to diffuse over an energy barrier into a primary minimum when it is greater than around $6-10k_BT_K$[10−12] (where $k_B$ is the Boltzmann constant and $T_K$ is the absolute temperature). Therefore, diminished aggregation and retention can be achieved when the energy barrier is increased above this level. Interaction energy calculations usually predict that the energy barrier between two negatively charged surfaces increases with increasing colloid size, lower ionic strength, high pH, more negatively charged systems, and/or lower Hamaker constants.[13]

Incompressible nanoscale roughness on mineral and metal surfaces will reduce colloid mass transfer to this surface by increasing the hydrodynamic slip.[14−16] In addition, interaction energies have frequently been demonstrated to be highly dependent on the incompressible nanoscale roughness proper-

Received: October 17, 2020
Revised: January 7, 2021
Published: January 20, 2021






https://dx.doi.org/10.1021/acs.langmuir.0c03029
*Langmuir* 2021, 37, 1501−1510

ties of both surfaces.[17] In particular, small amounts of incompressible nanoscale roughness protrusions that are specific to a colloid or porous medium[9,14,15,17,18] have been shown to dramatically decrease the magnitudes of the primary minimum, energy barrier height, and the secondary minimum,[19−29] especially when nanoscale roughness occurs on both interacting surfaces.[12,30] Furthermore, the influence of incompressible nanoscale roughness will change with the solution chemistry, the colloid size, the surface charges, and the water velocity.[12,16,28,31] Theoretical calculations have demonstrated that specific incompressible nanoscale roughness properties can greatly diminish colloid retention and aggregation, even when interactions for smooth surfaces are predicted to be favorable.[12,32] Spatial variability of incompressible roughness properties can explain why limited amounts of colloid aggregation and retention can occur.[17,31,33]

Compressible roughness may also occur on natural or engineered surfaces because of the adsorption of organic compounds such as polymers, surfactants, proteins, biological exudates, and humic materials.[5] These macromolecular coatings can exhibit different configurations on a surface depending on its curvature and the adsorbed layer properties (e.g., molecular weight, adsorption density, and layer thickness).[5,34−36] Organic layers on surfaces frequently exhibit nonuniform or incomplete surface coverage, so that portions of the underlying surface are likely to be exposed.[5] For example, globular proteins and polyelectrolytes are known to create patchy coatings.[37−40] Molecular coatings can either enhance or inhibit colloid aggregation and retention behavior. Enhanced colloid interactions have been attributed to charge neutralization or bridging of macromolecules.[5] In contrast, inhibited aggregation or retention has been explained by an increase in repulsive electrostatic, steric, or electrosteric interactions.[41−43]

Suspensions of NPs are normally stabilized by adsorption of organic compounds on their surface.[4,5,44] The enhanced stability of NPs with organic coatings has typically been attributed to steric effects when adsorbed organic layers overlap.[3] Indeed, interaction energy calculations that have been extended to include steric interactions predict that the energy barrier dramatically increases, and the primary minimum is eliminated when organic layers overlap.[4] However, NP suspensions that are stabilized by adsorbed organics frequently show various amounts of aggregation and retention that cannot be explained by steric effects.[18,45−48] One plausible explanation that will be investigated in this work is that the interaction energy profiles have been altered by compressible nanoscale roughness from adsorbed organic layers.[49] However, previous research has not yet simultaneously considered the influence of both steric and incompressible and/or compressible roughness effects on interaction energies. Furthermore, the relative importance of steric and roughness effects on colloid aggregation and retention has not been determined.

The retention of NPs and colloids have been reported to become stronger and more irreversible over time.[50−60] This implies that the strength of the adhesive interaction has increased with the residence time on a surface. Some researchers have attributed this to the formation of chemical bonds[55,56] when the separation distance approaches the size of molecules. Others indicate that an increase in the residence time is associated with an increase in the probability to diffuse into a deeper minimum in the interaction energy.[33,60,61] However, the potential role of adsorbed organic coatings and surface roughness on changes in the adhesive interaction has not yet been considered. It should be noted that consideration of steric interaction predicts that the energy barrier will increase when the organic layer is compressed or deformed.[34] Conversely, compression of an organic layer is also expected to decrease the compressible roughness height and increase the contact area between interacting surfaces. However, no published research to date has investigated the role of changing compressible surface roughness properties during aging on the strength of the adhesive interaction.

This research aims to theoretically investigate the influence of compressible and incompressible roughness on colloid aggregation and retention. This is achieved by considering the influence of steric interactions and nanoscale roughness on interaction energies. Furthermore, the potential role of changing roughness properties when organic coatings are compressed is addressed for the first time. Results from this work highlight the need to consider steric stabilization, incompressible nanoscale roughness, and changes in compressible nanoscale roughness properties to explain experimental observations of colloid retention, release, and aggregation.

## MATERIALS AND METHODS

**Interaction Energies for Homogeneous Surfaces.** The total interaction energy between a colloid and the solid water interface (SWI) ($\Phi_s$, M L$^2$ T$^{-2}$ where M, L, and T denote units of mass, length, and time, respectively) that are smooth and chemically homogeneous is assumed to be the sum of electrostatic, van der Waals, Born repulsion, and steric interaction energies as

$$\Phi_s(h) = \Phi^{el}(h) + \Phi^{vdW}(h) + \Phi^{Born}(h) + \Phi^{steric}(h) \quad (1)$$

where $h$ is the separation distance between the two surfaces, and $\Phi^{el}$ [M L$^2$ T$^{-2}$], $\Phi^{vdW}$ [M L$^2$ T$^{-2}$], $\Phi^{Born}$ [M L$^2$ T$^{-2}$], and $\Phi^{steric}$ [M L$^2$ T$^{-2}$] are the electric double layer, van der Waals, Born, and steric interaction energies, respectively. The value of $\Phi_s$ was made dimensionless by dividing by the product of the $k_B$ and $T_K$.

The value of $\Phi^{el}$ was determined using the constant surface potential interaction expression of Hogg et al.[62] for a sphere-plate interaction as follows

$$\Phi^{el}(h) = \pi\varepsilon\varepsilon_o r_c\left\{2\zeta_c\zeta_s \ln\left[\frac{1+\exp(-\kappa h)}{1-\exp(-\kappa h)}\right] + (\zeta_c^2+\zeta_s^2)\ln[1-\exp(-2\kappa h)]\right\} \quad (2)$$

where $\varepsilon$ (dimensionless) is the dielectric constant of the medium, $\varepsilon_0$ [M$^{-1}$ L$^{-3}$ T$^4$ A$^2$, where A denotes ampere] is the permittivity in a vacuum, $r_c$ [L] is the colloid radius, $\zeta_c$ [M L$^2$ T$^{-3}$ A$^{-1}$] is the zeta potential of the colloid, $\zeta_s$ [M L$^2$ T$^{-3}$ A$^{-1}$] is the zeta potential of the solid, and $\kappa$ [L$^{-1}$] is the Debye−Huckel parameter. Unless otherwise noted, $\zeta_c$ = −49 mV, $\zeta_s$ = −22 mV, and solution IS = 10 mM NaCl.[63]

The value of $\Phi^{vdW}$ for a retarded sphere-plate interaction was determined using the expression by Gregory[64] as follows

$$\Phi^{vdW}(h) = \frac{-A_{cws}r_c}{6h}\left[1+\frac{14h}{\lambda}\right]^{-1} \quad (3)$$

where $A_{cws}$ [M L$^2$ T$^{-2}$] is the combined Hamaker constant of the colloid−water−solid system that was taken to be 6.5 × 10$^{-21}$ J,[65,66] and $\lambda$ is a characteristic wavelength that was taken as 100 nm.[64]

The value of $\Phi^{Born}$ was calculated from Oliveira[67] for sphere-plate interactions as follows

$$\Phi^{Born}(h) = \frac{A_{cws}r_c h_0^{\,6}}{168h^7} \quad (4)$$

where $h_0$ [L] is the value of the closest approach that was taken to be 0.157 nm.[68] The steric interaction because of the presence of


https://dx.doi.org/10.1021/acs.langmuir.0c03029
Langmuir 2021, 37, 1501−1510

adsorbed organic coating was determined using theory from Alexander[69] and de Gennes[70] as follows

$$\Phi^{\text{steric}}(h \le H) = -\int_{\infty}^{h} F^{\text{steric}}(h)\mathrm{d}h$$

$$\Phi^{\text{steric}}(h > H) = 0 \quad (5)$$

where $F^{\text{steric}}$ [M L T$^{-2}$] is the steric force and $H$ [L] is the thickness of the adsorbed organic coating. The value of $H$ equals the sum of the adsorbed layer thickness on the colloid and the SWI,[3] and $F^{\text{steric}}$ is given by Byrd and Walz[71] as follows

$$F^{\text{Steric}}(h \le H) = 2\pi r_c\left(\frac{k_B T_K}{\sigma^3}\right)\left(\frac{4H}{5}\left[\left(\frac{H}{h}\right)^{5/4} - 1\right] + \frac{4H}{7}\left[\left(\frac{h}{H}\right)^{7/4} - 1\right]\right) \quad (6)$$

where $\sigma$ [L] is the distance between the organic chains on the surface and is taken to be 5 nm[45] on both surfaces.

Equations 1−6 may also be adapted to describe colloid−colloid interactions by replacing $r_c$ with $r_{c1}r_{c2}/(r_{c1} + r_{c2})$, where the radii of the two colloids are $r_{c1}$ and $r_{c2}$, respectively. Limitations in the applicability of these interaction energy expressions are given in the literature.[62,64,67,69−71] Equations 1−6 implicitly assume that the electric double layer, van der Waals, and Born interactions are not influenced by the geometry of adsorbed organics in the region $h \le H$.

**Interaction Energies for Heterogeneous Surfaces.** The approach of Bradford et al.[12] was used to account for the influence of nanoscale roughness on the interaction energy between a spherical colloid suspended in a monovalent electrolyte solution and a planar solid surface or another colloid. In this case, the mean dimensionless interaction energy between a colloid and SWI that contains nanoscale roughness on both surfaces ($\Phi$) can be determined as a linear combination of interaction energies for the various nanoscale roughness components as follows[12]

$$\Phi(h) = a_{r1}\Phi_S(h) + a_{r2}\Phi_s(h - h_{cr}) + a_{r3}\Phi_s(h - h_{sr}) + a_{r4}\Phi_s(h - h_{cr} - h_{sr}) \quad (7)$$

where $h_{sr}$ and $h_{cr}$ are the surface roughness heights on the SWI and colloid, respectively, and $a_{r1}$ [-], $a_{r2}$ [-], $a_{r3}$ [-], and $a_{r4}$ [-] are constants that determine the contributions of the various possible roughness combinations that are equal to

$$a_{r1} = (1 - f_{sr})(1 - f_{cr})$$

$$a_{r2} = (1 - f_{sr})f_{cr}$$

$$a_{r3} = f_{sr}(1 - f_{cr})$$

$$a_{r4} = f_{sr}f_{cr} \quad (8)$$

where $f_{sr}$ and $f_{cr}$ are the fractions of the electrostatic zone of influence occupied by roughness heights $h_{sr}$ and $h_{cr}$, respectively. The value of $h$ in eq 7 is the separation distance from the leading face of the underlying surface of the colloid to the center of the zone of electrostatic influence on the underlying surface of the SWI. Equations 7 and 8 are consistent with previous studies that have demonstrated that the mean interaction energy for heterogeneous surfaces can be determined as a linear combination of interaction energies associated with the various heterogeneity types.[23,24,26] The lower limit for $f_{sr}$, $f_{cr}$, $h_{sr}$, and $h_{cr}$ is 0. The upper limit for $f_{sr}$ and $f_{cr}$ is 1, whereas there is no theoretical upper limit for $h_{sr}$ and $h_{cr}$. However, the contribution of the underlying surface to the interaction energy rapidly approaches zero when $h_{sr}$ or $h_{cr}$ is greater than around 100−200 nm.

It should be mentioned that eqs 7 and 8 have previously been extended to account for random distributions of binary heterogeneity of zeta potential, Hamaker constant, and/or hydrophobicity on the SWI and/or the colloid.[12,30] The same heterogeneity was assumed to occur on the roughness pillars and underlying surface of a colloid or SWI in these publications. In contrast, separate zeta potential properties were sometimes used for the roughness pillars and the underlying surface of a colloid or SWI in this work. In this case, the first, second, third, and fourth terms on the right-hand side of eq 7 employ zeta potential values for the underlying surface of the SWI and colloid, the underlying surface of the SWI and the roughness pillars on the colloid, the roughness pillars on the SWI and the underlying surface of the colloid, and the roughness pillars of the SWI and colloid, respectively. This same approach may also be employed to account for differences in the Hamaker constant or hydrophobicity of the underlying surface and roughness pillars as well. Unless otherwise noted, the properties of the underlying surface and the roughness pillars were assumed to be the same.

Bradford et al.[12] previously assumed constant values of $h_{sr}$, $h_{cr}$, $f_{sr}$, and $f_{cr}$ and, therefore, implicitly neglected roughness deformation or compression. In the present study, values of $h_{sr}$, $h_{cr}$, $f_{sr}$, and $f_{cr}$ change with compression for electrostatic, van der Waals, and Born interactions. Equations 7 and 8 assume that roughness on the SWI and colloid do not overlap so that the lateral components of the interaction force can be neglected or canceled out. In this case, the minimum separation distance ($h_{min}$) is, therefore, $h_o + (1 - \omega_{sd})h_{sri} + (1 - \omega_{cd})h_{cri}$, where $h_{sri}$ and $h_{cri}$ denote values of $h_{sr}$ and $h_{cr}$ before compression, and $\omega_{sd}$ and $\omega_{cd}$ are parameters that determine whether $h_{sri}$ and $h_{cri}$, respectively, are incompressible ($\omega = 0$) or compressible ($\omega = 1$). Compression occurs when $h_{min} < h \le (h_{sri} + h_{cri} + h_o)$ and $h_{sr}$, $h_{cr}$, $f_{sr}$, and $f_{cr}$ change as follows

$$h_{sr} = (1 - \omega_{sd})h_{sri} + (h - h_{min})\frac{\omega_{sd}h_{sri}}{\omega_{sd}h_{sri} + \omega_{cd}h_{cri}} \quad (9)$$

$$h_{cr} = (1 - \omega_{cd})h_{cri} + (h - h_{min})\frac{\omega_{cd}h_{cri}}{\omega_{sd}h_{sri} + \omega_{cd}h_{cri}} \quad (10)$$

$$f_{sr} = f_{sri}\frac{h_{sri}}{h_{sr}} \quad (11)$$

$$f_{cr} = f_{cri}\frac{h_{cri}}{h_{cr}} \quad (12)$$

where $f_{sri}$ and $f_{cri}$ denote values of $f_{sr}$ and $f_{cr}$ before compression ($h > h_{sri} + h_{cri} + h_o$), respectively. Note that the first term on the right-hand side of eqs 9 and 10 determines if $h_{sri}$ and $h_{cri}$ are incompressible, whereas the second term linearly scales the compressible roughness heights with $h-h_{min}$ when $(h - h_{min}) < (h_o + \omega_{sd}h_{sri} + \omega_{cd}h_{cri})$. Equations 11 and 12 assume that the volume of the roughness is constant during compression (completely elastic), and a decrease in the roughness height during compression, therefore, leads to a corresponding increase in the roughness fraction (e.g., related to the surface area of the roughness). Figure 1a presents an illustration of changes in the roughness height and fraction during compression.

Steric interactions only occur when nanoscale roughness is compressed. In this case, the value of $H$ in eqs 5 and 6 is equal to 0, $\omega_{cd}$ $h_{cri}$, $\omega_{sd}$ $h_{sri}$, and $\omega_{cd}$ $h_{cri}$+ $\omega_{sd}$ $h_{sri}$ for the first, second, third, and fourth terms on the right-hand side of eq 7, respectively. Steric interactions already explicitly consider compression and were therefore not further modified for changes in the compressible roughness height and fraction. The influence of roughness on steric interactions was, therefore, only considered for the incompressible roughness proportion by setting $h_{sr}$ and $h_{cr}$ in eq 7 equal to $(1 - \omega_{sd})$ $h_{sri}$ and $(1 - \omega_{cd})h_{cri}$, respectively.

Figure 1 presents an illustration of the various types of surface roughness that we will consider in this manuscript because of the presence of adsorbed organic compounds and/or rough mineral or colloid surfaces. Equations 1−12 allow the influence of these various roughness types to be systematically investigated on one or two surfaces when considering double layer, van der Waals, Born, and/or steric interactions. Specific interaction energy calculations were conducted to explore the roles of (i) incompressible roughness (Figure 1b); (ii) compressible roughness in the absence of steric



https://dx.doi.org/10.1021/acs.langmuir.0c03029
Langmuir 2021, 37, 1501−1510

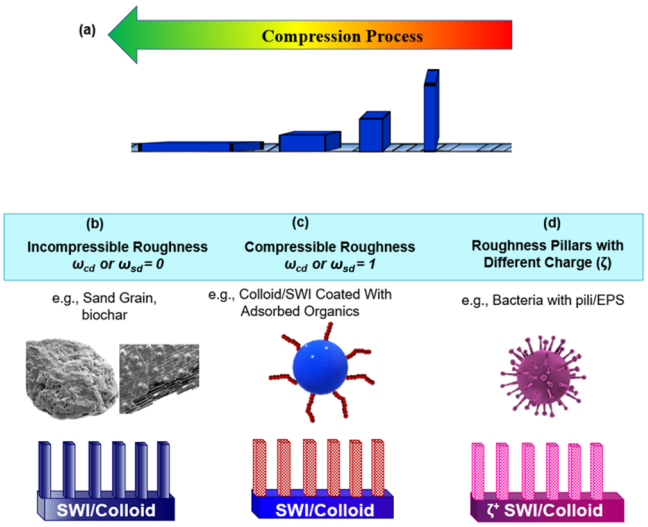


**Figure 1.** Illustration of the compression process of a rough surface (a), incompressible roughness (b), compressible roughness (c), and roughness with a different charge than the underlying surface (d).

interaction (Figure 1c); (iii) compressible roughness in the presence of steric interactions (Figure 1c); (iv) incompressible roughness on the SWI (Figure 1b) and compressible roughness on the colloid (Figure 1c); and (v) compressible roughness pillars with a different charge than the underlying surface (Figure 1d). In addition, other factors such as colloid size, solution ionic strength, zeta potential of the SWI, and zeta potential of the roughness on the SWI were investigated. Parameter values that were used in these calculations are provided below and in the figure captions.

The interaction energy profiles were plotted in this paper as a function of $h-h_{min}$ to improve the presentation and interpretation of results. Note that $h-h_{min}$ is the separation distance from the tops of the incompressible roughness heights on both the SWI and the colloid. All interaction energy profiles were analyzed to determine the energy barrier height and the depths of the secondary and primary minima.

## RESULTS AND DISCUSSION

**Incompressible Nanoscale Roughness.** Figure 2a presents plots of Φ as a function of $h-h_{min}$ for a smooth NP ($h_{cri}$ = 0 nm, $\omega_{cd}$ = 0, and $f_{cri}$ = 0) with a diameter of 100 nm when the IS = 10 mM and the SWI exhibits different fractions ($f_{sri}$ = 0.01, 0.1, 0.25, 0.50, and 1.00) of incompressible roughness (Figure 1b; $\omega_{sd}$ = 0) with a height of 10 nm ($h_{sri}$ = 10 nm). Note that a decrease in $f_{sri}$ produces a reduction in the energy barrier height and the primary minimum depth. This behavior has been previously observed[19−21,23−29] and attributed to the decrease in the contribution of roughness pillar tops at smaller separation distances to Φ; for example, the underlying surface at the bottom of the roughness plays a more important role but has a smaller magnitude because it is at a larger separation distance. The value of $h_{sri}$ has also been shown to influence the calculated interaction energy profile when $f_{sri}$ is relatively small (e.g., <25%), but the influence of $h_{sri}$ is generally less important than $f_{sri}$.[17] It should also be mentioned that roughness parameters for a rough NP and smooth SWI will have a similar influence on interaction energies as for a smooth NP and rough SWI.[12] Subsequently, calculations exploring the influence of the roughness parameter mainly focus on changes in $f_{sri}$.

Figure 2b presents plots of Φ as a function of $h-h_{min}$ for a NP with a 100 nm diameter and SWI that both exhibit

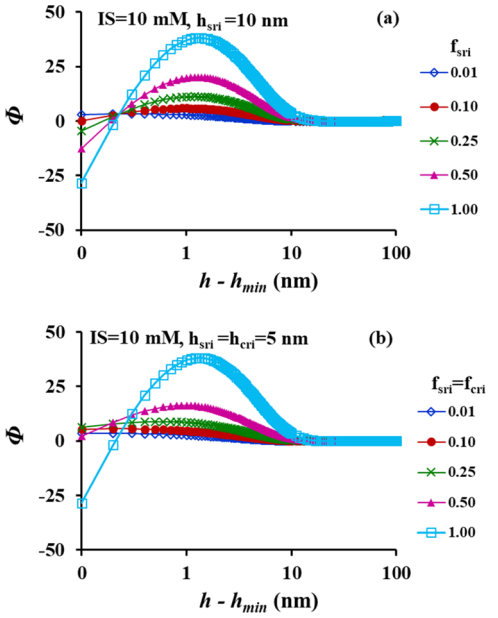


**Figure 2.** Plots of the dimensionless interaction energy (Φ) as a function of separation distance ($h-h_{min}$) for a 100 nm diameter particle when the IS = 10 mM and the nanoscale roughness was incompressible. In (a), particle was smooth ($h_{cri}$ = 0 nm, $\omega_{cd}$ = 0, and $f_{cri}$ = 0), and the SWI had the following roughness properties $h_{sri}$ = 10 nm, $\omega_{sd}$ = 0, and $f_{sri}$ = 0.01, 0.1, 0.25, 0.50, and 1.00. In (b), both surfaces were rough and had the following properties $\omega_{sd}$ = $\omega_{cd}$ = 0, $h_{sri}$ = $h_{cri}$ = 5 nm, and $f_{sri}$ = $f_{sri}$ = 0.01, 0.1, 0.25, 0.50, and 1.00.

incompressible roughness (Figure 1b; $\omega_{sd}$ = $\omega_{cd}$ = 0) when the IS = 10 mM, $h_{sri}$ = $h_{cri}$ = 5 nm, and different roughness fractions ($f_{sri}$ = $f_{cri}$ = 0.01, 0.1, 0.25, 0.50, and 1.00) are considered. Note that the same total roughness height ($h_{sri}$ + $h_{cri}$ = 10 nm) was considered in these calculations as for Figure 2a. Similar to Figure 2a, the energy barrier height and the depth of the primary minimum were decreased with smaller values of $f_{sri}$ = $f_{cri}$. In contrast to Figure 2a, the energy barrier was smaller, and the attractive depth of the primary minimum was eliminated. This difference occurs because the interacting surface on the pillar tops of the SWI and the NP was smaller when two surfaces exhibit roughness. Similar interaction energy results for roughness on two surfaces have appeared in the literature previously.[12,30]

**Compressible Nanoscale Roughness without Steric Interactions.** Figure 3a presents plots of Φ as a function of $h-h_{min}$ for a smooth NP ($h_{cri}$ = 0 nm, $\omega_{cd}$ = 0, and $f_{cri}$ = 0) with a diameter of 100 nm when the IS = 10 mM and the SWI exhibits different fractions ($f_{sri}$ = 0.01, 0.1, 0.25, 0.50, and 1.00) of compressible (Figure 1c; $\omega_{sd}$ = 1) roughness with a height of 10 nm ($h_{sri}$ = 10 nm). In this case, steric interactions were neglected, and a decrease in $h_{sr}$ during compression resulted in a corresponding increase in $f_{sr}$ that alters the contributions of electrostatic, van der Waals, and Born interactions when $h-h_{min} \leq$ 10 nm (Figure 1a). The influence of roughness on the SWI before compression is seen in this figure when $h-h_{min}$ > 10 nm. Similar to Figure 1a, smaller values of $f_{sri}$ produce greater reductions in the energy barrier height. The influence of compressible roughness becomes apparent when $h-h_{min} \leq$ 10 nm. Notice that the interaction energy profile approaches the smooth incompressible surface (e.g., Figure 1a when $f_{sri}$ = 1) when $f_{sri}$ is small. Conversely, compression does not alter the primary minimum depth when $f_{sri}$ = 1 and $h-h_{min} \leq$ 10 nm


https://dx.doi.org/10.1021/acs.langmuir.0c03029
Langmuir 2021, 37, 1501−1510

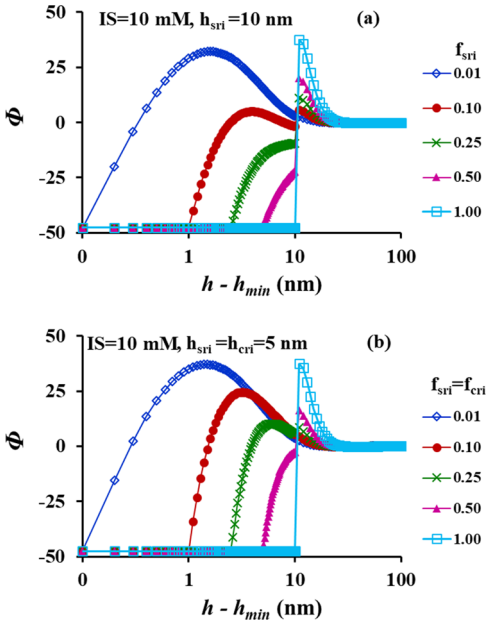


**Figure 3.** Plots of the dimensionless interaction energy ($\Phi$) as a function of separation distance ($h-h_{min}$) for a 100 nm diameter particle when the IS = 10 mM, nanoscale roughness was compressible, and steric interaction was absent. In (a), particle was smooth ($h_{cri}$ = 0 nm, $\omega_{cd}$ = 1, and $f_{cri}$ = 0), and the SWI had the following roughness properties $h_{sri}$ = 10 nm, $\omega_{sd}$ = 1, and $f_{sri}$ = 0.01, 0.1, 0.25, 0.50, and 1.00. In (b), both surfaces were rough and had the following properties $\omega_{sd}$ = $\omega_{cd}$ = 1, $h_{sri}$ = $h_{cri}$ = 5 nm, and $f_{sri}$ = $f_{sri}$ = 0.01, 0.1, 0.25, 0.50, and 1.00.

because the roughness fraction does not change. Intermediate values of 0.01 < $f_{sri}$ < 1 when $h-h_{min} \leq 10$ nm tend to produce a decrease in the depth of the primary minimum during compression because of an increase in $f_{sr}$ until $f_{sr}$ = 1. Interaction energy profiles that show an increase in the strength of the primary minimum with further decreases in the separation distance are favorable for compression (e.g., $f_{sri}$ = 0.25 and 0.5), whereas those that exhibit an energy barrier (e.g., $f_{sri}$ = 0.01 and 0.1) are unfavorable for continued compression. This important result highlights that compression/deformation of surface roughness when $f_{sri}$ = 0.25 and 0.5 may at least partially explain the reported increase in the strength of colloid and NP interactions with time.[55−60] It also provides a potential alternative explanation for repulsion when surface structures ($f_{sri}$ = 0.01 and 0.1) are compressed that has typically been attributed to steric repulsion.[3−5]

Figure 3b presents plots of $\Phi$ as a function of $h-h_{min}$ for a NP with a 100 nm diameter and SWI that both exhibit compressible roughness (Figure 1c; $\omega_{sd}$ = $\omega_{cd}$ = 1) when the IS = 10 mM, $h_{sri}$ = $h_{cri}$ = 5 nm, and different roughness fractions ($f_{sri}$ = $f_{cri}$ = 0.01, 0.1, 0.25, 0.50, and 1.00) are considered. Note that steric effects were neglected in these calculations. The influence of roughness on the NP and SWI before compression is seen in this figure when $h-h_{min}$ > 10 nm. In this case, an enhanced reduction in the energy barrier happens when roughness occurs on two surfaces (Figure 3b) in comparison to one (Figure 3a). The influence of compressible roughness is apparent when $h-h_{min} \leq 10$ nm. Similar to Figure 3a, the interaction energy profile approaches smooth, incompressible surfaces when $f_{sri}$ = $f_{cri}$ = 0 and a smooth, compressible surfaces when $f_{sri}$ = $f_{cri}$ = 1. In contrast to Figure 3a, results are more sensitive to the roughness fraction when it occurs on two ($f_{sri}$ = $f_{cri}$ in Figure 3b) in comparison to one ($f_{sri}$ in Figure 3a) surface. In particular, interaction energy profiles approach the smooth, incompressible surface for smaller roughness fractions ($f_{sri}$ = $f_{cri}$), and conditions are generally less favorable for continued compression because they produce larger energy barriers when $h-h_{min} \leq 10$.

**Compressible Nanoscale Roughness with Steric Interactions.** Additional interaction energy calculations were conducted to further investigate the combined influence of compressible roughness and steric interactions. Figure 4a

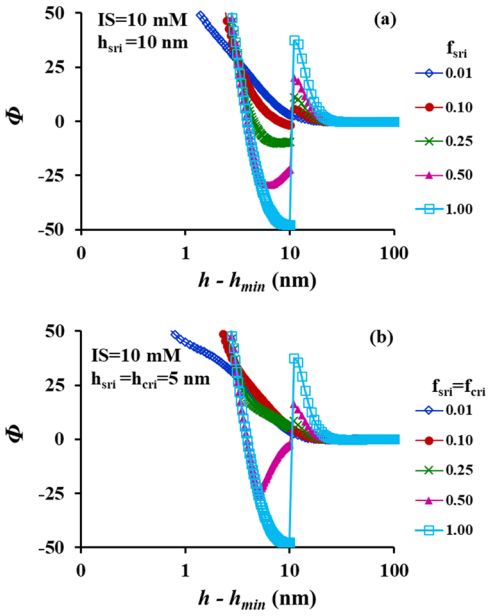


**Figure 4.** Plots of the dimensionless interaction energy ($\Phi$) as a function of separation distance ($h-h_{min}$) for a 100 nm diameter particle when the IS = 10 mM, nanoscale roughness was compressible, and steric interaction was present. In (a), particle was smooth ($h_{cri}$ = 0 nm, $\omega_{cd}$ = 1, and $f_{cri}$ = 0) and the SWI had the following roughness properties $h_{sri}$ = 10 nm, $\omega_{sd}$ = 1, and $f_{sri}$ = 0.01, 0.1, 0.25, 0.50, and 1.00. In (b), both surfaces were rough and had the following properties $\omega_{sd}$ = $\omega_{cd}$ = 1, $h_{sri}$ = $h_{cri}$ = 5 nm, and $f_{sri}$ = $f_{sri}$ = 0.01, 0.1, 0.25, 0.50, and 1.00.

presents plots of $\Phi$ as a function of $h-h_{min}$ when steric interactions are considered for a smooth NP ($h_{cri}$ = 0 nm, $\omega_{cd}$ = 0, and $f_{cri}$ = 0) with a diameter of 100 nm when the IS = 10 mM and the SWI exhibits different fractions ($f_{sri}$ = 0.01, 0.1, 0.25, 0.50, and 1.00) of compressible (Figure 1b; $\omega_{sd}$ = 1) roughness with a height of 10 nm ($h_{sri}$ = 10 nm). Note that Figures 3a and 4a are identical when $h-h_{min}$ > 10 nm, which reflect the influence of roughness before compression. The combined influence of compressible roughness and steric interactions becomes apparent when $h-h_{min} \leq 10$ nm. The role of compressible roughness tends to control the interaction energy profile during the initial phase of deformation (e.g., when 8 < $h-h_{min} \leq 10$ nm), but then steric repulsion rapidly increases to dominate the profile. The combined influence of these effects produces a small energy barrier exterior to the initial roughness height, a shallow primary minimum interior to the initial roughness height, and a rapidly increasing energy barrier with further compression due to steric effects. Similar to incompressible roughness (Figure 2a), the depth of the primary minimum increases with $f_{sri}$. In contrast, the primary minima for compressible roughness occur at much larger


https://dx.doi.org/10.1021/acs.langmuir.0c03029
Langmuir 2021, 37, 1501−1510

values of $h-h_{min}$ than for incompressible roughness. The presence of shallow primary minima on compressible surfaces can explain why limited amounts of aggregation and retention have been commonly observed for NPs in the presence of compressible organic (polymers, surfactants, and humic material) coatings.[18,45−48] The presence of patchy or incomplete coverage of an adsorbed organic layer could also locally eliminate steric effects to create retention, but this hypothesis cannot explain observed differences in stability and retention with alterations of solution or solid-phase chemistry.[10−14]

Figure 4b presents plots of Φ as a function of $h-h_{min}$ when steric interactions are considered for a NP with a 100 nm diameter and SWI that both exhibit compressible roughness (Figure 1b; $\omega_{sd} = \omega_{cd} = 1$), the IS = 10 mM, $h_{sri} = h_{cri} = 5$ nm, and $f_{sri} = f_{cri} = 0.01$, 0.1, 0.25, 0.50, and 1.00. Results in Figure 4b are identical to Figure 4a when $h-h_{min} > 10$ nm, but they start to diverge after a few nm of compression because of the dominating influence of repulsive steric interactions. Similar to Figure 4a, compressible roughness may sometimes produce a shallow primary minimum (e.g., $f_{sri} = f_{cri} = 0.50$) at separation distances just interior to the initial compressible height ($h_{sri} + h_{cri}$) before steric interactions dominate the profile. In contrast to Figure 4a, shallow primary minima occur for larger roughness fractions when roughness occurs on two ($f_{sri}$ and $f_{cri}$) than one (only $f_{sri}$) surface.

**Compressible Nanoscale Roughness on NP and Incompressible Roughness on SWI.** Additional interaction energy calculations were conducted to explore the influence of a 100 nm diameter NP with compressible roughness (Figure 1c; $\omega_{cd} = 1$; $f_{cri} = 0.5$) on a SWI with different incompressible roughness (Figure 1b; $\omega_{sd} = 0$) properties when the solution IS = 10 mM. Figure 5a presents plots of Φ as a function of $h-h_{min}$ when values of $f_{sri}$ (0.01, 0.1, 0.25, 0.50, and 1.00) varied and $h_{sri} = h_{cri} = 5$ nm. The interaction profiles exhibit three distinct regions. The influence of roughness before compression occurs when $h-h_{min} > 5$ nm. In this case, roughness reduces the energy barrier height and the depth of the primary minimum. The compression of the roughness on the NP altered the depth of the primary minimum when $2.5 < h-h_{min} \leq 5$ nm. Larger values of $f_{sri} = 0.25$, 0.5, and 1 were energetically favorable for compression, whereas smaller values of $f_{sri} = 0.01$ and 0.1 were unfavorable for compression. Steric repulsion dominated the interaction energy profile when $h-h_{min} \leq 2.5$ nm and increased with $f_{sri}$ in this region. These results indicate that small incompressible roughness fractions on the SWI will drastically reduce the steric repulsion.

Figure 5b shows plots of Φ as a function of $h-h_{min}$ when incompressible $h_{sri}$ (1, 2.5, 5.0, 7.5, and 9 nm) and compressible $h_{cri} = 10 - h_{sri}$ are varied, and $f_{sri} = f_{cri} = 0.5$. Note that the location of the energy barrier and primary minimum occurs at larger values of $h-h_{min}$ when $h_{sri}$ decreases and $h_{cri}$ increases, even though the total value of $h_{sri} + h_{cri}$ always equaled 10 nm. This occurs because the value $h_{min}$ increases with the incompressible $h_{sri,}$ and the energy barrier occurs just exterior to the compressible roughness $h_{cri}$. Consequently, changes in the compressible roughness height will alter the location of these parameters. However, the energy barrier height was not much influenced by whether the roughness occurs on the NP or the SWI. Compressible roughness initially dominates the interaction energy profiles at separation distances just interior to the compressible roughness $h_{cri}$ and then steric repulsions become controlling at smaller

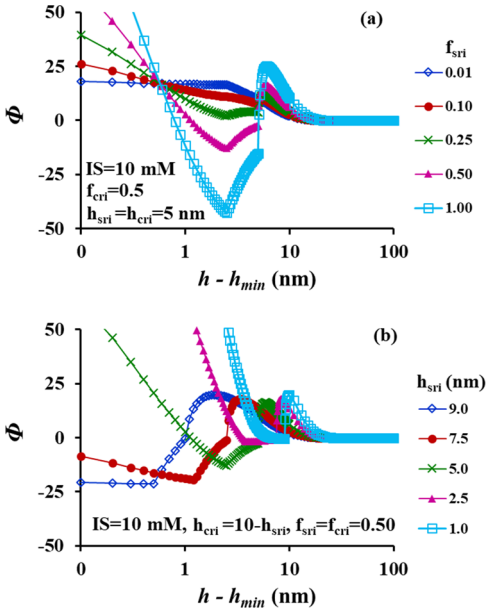


**Figure 5.** Plots of the dimensionless interaction energy (Φ) as a function of separation distance ($h-h_{min}$) for a 100 nm diameter particle when the IS = 10 mM, nanoscale roughness was compressible on the particle ($\omega_{cd} = 1$ and $f_{cri} = 0.5$) and incompressible ($\omega_{sd} = 0$) on the SWI, and steric interaction was considered. In (a), values of $f_{sri}$ (0.01, 0.1, 0.25, 0.50, and 1.00) were varied and $h_{sri} = h_{cri} = 5$ nm. In (b), values of $h_{sri}$ (1, 2.5, 5.0, 7.5, and 9 nm) and $h_{cri} = 10 - h_{sri}$ were varied, and $f_{sri} = f_{cri} = 0.5$.

separation distances. Compressible roughness produced deeper primary minima when $h_{cri}$ was smaller because of a reduction in steric repulsion. Conversely, steric repulsion is greater for larger values of compressible $h_{cri,}$ and this produces shallower primary minima.

**Other Factors Influencing the Effect of Compressible Nanoscale Roughness.** It should be mentioned that effects of incompressible roughness on interaction energy profiles have been previously demonstrated to be a function of the colloid size, the solution chemistry, the surface zeta potentials, and the roughness height.[20−29,45,58,72,73] These same factors also influence interaction energy profiles when the nanoscale roughness is compressible and steric effects are considered. For example, Figures S1 and S2 show that the energy barrier height increases and the depth of the primary minimum increases with increasing colloid diameter (IS = 10 mM) and decreasing IS (NP diameter of 100 nm), respectively, when the colloid is smooth, $h_{sri} = 10$ nm, $\omega_{sd} = 1$, $f_{sri} = 0.25$ in Figure S1 and $f_{sri} = 0.5$ in Figure S2. Note in Figure S2 that zeta potentials were assumed to be independent of the IS so that effects of changes in the double layer thickness could be more clearly identified. Figure S3 presents plots of the interaction energy profiles for similar conditions, except that values of $\zeta_s$ were varied from 10, 0, −10, −25, and −50 mV while $\zeta_c$ was kept at −22 mV. The energy barrier height increased, and the depth of the primary minimum became shallower with decreasing (more negative) $\zeta_s$ because of greater electrostatic repulsion. Figure S4 shows plots of the interaction energy profiles for the same conditions as in Figure S3, but when $f_{sri} = 0.10$, the zeta potential of the underlying surface of the SWI was set to −49 mV and the zeta potential of the roughness pillars on the SWI was set to 10, 0, −10, −25, and −50 mV (Figure 1c). Similar to Figure S3, a decrease (more negative) in the zeta potential of the roughness


https://dx.doi.org/10.1021/acs.langmuir.0c03029
Langmuir 2021, 37, 1501−1510

pillars increased the energy barrier height, and the depth of the primary minimum became shallower. However, these effects on the interaction energy profile were reduced compared to when the zeta potential of the entire SWI was altered (Figure S3). Results in Figure S4 approach those of Figure S3 as $f_{sri}$ goes to 1.

Figure S5 shows the interaction energy profile for a smooth 100 nm diameter NP in 10 mM solution when it approached a SWI with incompressible roughness (Figure S5a), compressible roughness without steric interactions (Figure S5b), and compressible roughness with steric interactions (Figure S5c). The roughness properties on the SWI were $f_{sri}$ = 0.25 and $h_{sri}$ = 2.5, 5, 10, 25, and 50 nm. Note that increasing $h_{sri}$ decreases the energy barrier in the presence of incompressible roughness in Figure S5a because of reduced repulsion from the underlying surface. This same effect is also seen exterior to the compressible roughness layer ($h-h_{min} > h_{sri}$) in Figure S5b,c. In contrast, an increase in $h_{sri}$ creates compression over a greater distance as it approaches the primary minimum of a smooth surface in Figure S5b. The strength of steric repulsion increases with $h_{sri}$ in Figure S5c, and this produces a shallower depth in the primary minimum that occurs interior to the compressible layer.

**Applications.** Table S1 summarizes published results from column studies examining the transport and retention of silver NPs (AgNPs) coated by a mixture of two non-ionic surfactants under different solution IS conditions (5, 10, 20, 40, and 50 mM) in clean quartz sand.[14] Significant amounts of AgNP retention occur in these systems; for example, the mass percentage of retained AgNPs on the sand ranged from 20.8% at IS = 5 mM to 100% at IS = 50 mM. Dimensionless interaction energy parameters (maximum energy, $\Phi_{max}$; depth of primary minimum interior to the compressible layer, $\Phi_{1min}$; and energy barrier exterior to the compressible layer, $\Phi_{bar}$) are also presented in Table S1 when considering different incompressible roughness fractions on the SWI ($f_{sri}$ = 0.01, 0.05, 0.1, 0.25, 0.5, and 1), $h_{sri}$ = 30 nm, and steric effect when a smooth AgNP with a 10 nm adsorbed surfactant layer is compressed.

Steric repulsion is predicted to create huge energies when the surfaces are assumed to be smooth, and the influence of compressible roughness on van der Waals and double layer interactions is neglected (Figure S6). In contrast to experimental observations (Table S1), no AgNP attachment is predicted under these conditions (there are no adhesive minima). Conversely, the value of $\Phi_{bar}$ decreases with increasing IS and for smaller values of $f_{sri}$ when considering the influence of AgNP compression, steric effects, and incompressible roughness on the SWI. Similar to experimental observations (Table S1), AgNP attachment in a primary minimum is possible for all IS conditions (e.g., when $\Phi_{bar} < 5-10$), but more roughness properties contribute to retention at higher IS. These predictions are consistent with the significant amounts of colloid retention that occurred in these systems.

The influence of binary roughness heterogeneity on the surface of the colloid and the SWI on interaction energies is accounted for in this work using a linear superposition approach. This is a simplification of the actual roughness of natural surfaces, which can exhibit great complexity and spatial variability.[16,20−25,45] Several approaches have been reported in the literature to account for more realistic surface roughness heterogeneity. For example, Bradford and Torkzaban[33] accounted for spatial variability in roughness properties on a surface by randomly sampling probability density functions for the incompressible roughness height and fraction and then calculated the interaction energy profile at 1000 locations using a linear superposition approach.[27] The mean and variance of the fraction of the surface area contributing to colloid retention were subsequently calculated from this information. This same method could also be easily implemented for compressible roughness with and without steric interactions, but the trends reported in this work would not change. Alternatively, the more computationally intensive surface element integration approach has been used to calculate interaction energy maps over a fractal representation of incompressible surface roughness.[32] Results from these calculations are qualitatively consistent with the simpler linear superposition approach, and atomic force microscope maps of measured roughness and adhesive forces across a surface under differing IS conditions,[9] for example, a reduction in the interaction energy profile occurs at the tops of roughness asperities that change with the solution IS. Surface element integration calculations have not yet been extended to consider the role of steric repulsion and compressible roughness but are also expected to be qualitatively consistent with the results presented in this work. Additional research is needed to resolve this issue entirely but is beyond the scope of this research.

## CONCLUSIONS

Colloid suspensions that have been stabilized by adsorbed organics such as surfactants, polymers, and humic compounds frequently show various amounts of aggregation and retention, even though steric interactions do not predict this behavior. Theory was developed to overcome this limitation by considering the roles of incompressible and compressible nanoscale roughness on interaction energy calculations. These calculations accounted for the electric double layer, retard van der Waals, Born, and steric interactions, as well as nanoscale roughness.

Nanoscale roughness was predicted to significantly influence the energy barrier height exterior to the compressible rough coating. In this case, a decrease in the roughness fraction produces a corresponding reduction in the energy barrier height because of a smaller interacting surface. Steric interactions and compression/deformation of the nanoscale roughness occur interior to the initial compressible roughness height. A decrease in the roughness height produces a corresponding increase in the roughness fraction in this region. The compression of nanoscale roughness may be energetically favorable or unfavorable depending on the roughness, steric, colloid, SWI, and solution chemistry properties. Smaller roughness fractions tended to produce conditions that were more energetically unfavorable for compression. Shallow primary minima were predicted to occur next to the interior side of the initial roughness height when repulsive steric interactions were considered. In this case, the primary minimum depth was predicted to be a strong function of the nanoscale roughness, colloid, SWI, and solution chemistry properties. Shallower primary minima tended to occur for smaller roughness fractions, larger roughness heights, smaller particle sizes, larger IS, and for more electrostatically repulsive conditions. Steric repulsion was reduced in the presence of incompressible roughness, especially for lower incompressible roughness fractions and smaller compressible roughness heights. Roughness effects on interaction energies were magnified when roughness occurred on both surfaces of the


https://dx.doi.org/10.1021/acs.langmuir.0c03029
Langmuir 2021, 37, 1501−1510

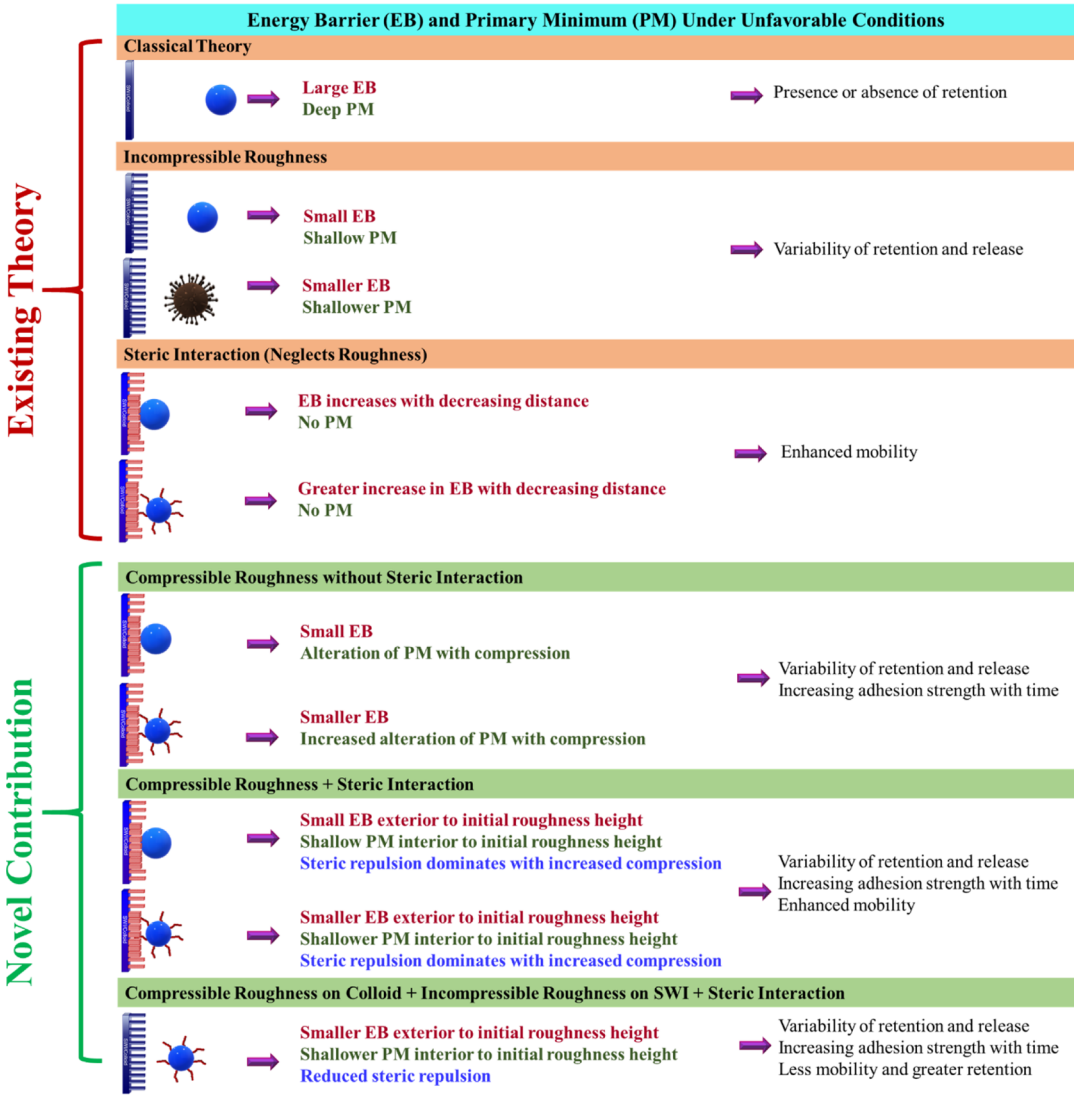


**Figure 6.** Schematic that illustrates the main findings and contributions of this work over previous literature.

colloid and the SWI, mainly due to decreased interacting surface area on the pillar tops.

Figure 6 presents a schematic that illustrates the main findings and contributions of this work over previous literature. Results in this study can explain limited amounts of aggregation and retention for colloids stabilized by adsorbed organic compounds. They can also provide a potential explanation for observed increases in particle adhesion strength with the residence time. The developed approach provides a valuable tool to improve the design of particles and surfaces for specific applications.

## ■ ASSOCIATED CONTENT

### Supporting Information

The Supporting Information is available free of charge at https://pubs.acs.org/doi/10.1021/acs.langmuir.0c03029.

Plots of the dimensionless interaction energy ($\Phi$) as a function of separation distance ($h-h_{min}$) for various roughness conditions in the presence or absence of steric interactions for different colloid diameters, ionic strengths, zeta potentials on the SWI, zeta potentials on the roughness, and roughness heights; experimental conditions and results from column experiments using quartz sand and surfactant-coated AgNPs under various IS conditions; and interaction energy parameters when considering different incompressible roughness fractions on the SWI and steric effects from the coated AgNP (PDF)

## ■ AUTHOR INFORMATION


### Corresponding Author

**Scott A. Bradford** − *USDA, ARS, SAWS Unit, Davis, California 95616, United States;* orcid.org/0000-0002-3260-2968; Phone: 951-224-7921.; Email: Scott.Bradford@usda.gov

### Authors

**Salini Sasidharan** − *USDA, ARS, SAWS Unit, Davis, California 95616, United States; Environmental Sciences Department, University of California, Riverside, California 92521, United States*

**Hyunjung Kim** − *Department of Mineral Resources and Energy Engineering, Jeonbuk National University, Jeonju, Jeonbuk 54896, Republic of Korea;* orcid.org/0000-0003-2115-6891




https://dx.doi.org/10.1021/acs.langmuir.0c03029
*Langmuir* 2021, 37, 1501−1510

**Allan Gomez-Flores** − *Department of Mineral Resources and Energy Engineering, Jeonbuk National University, Jeonju, Jeonbuk 54896, Republic of Korea;* orcid.org/0000-0003-0532-7232

**Tiantian Li** − *Department of Soil and Water Sciences, China Agricultural University, Beijing 100193, China*

**Chongyang Shen** − *Department of Soil and Water Sciences, China Agricultural University, Beijing 100193, China;* orcid.org/0000-0002-2517-3472

Complete contact information is available at: https://pubs.acs.org/10.1021/acs.langmuir.0c03029

### Notes

The authors declare no competing financial interest.

## ■ ACKNOWLEDGMENTS

This research was supported by the USDA, ARS, National Program 212.

## ■ REFERENCES

(1) Colvin, V. L. The potential environmental impact of engineered nanomaterials. *Nat. Biotechnol.* **2003**, *21*, 1166−1170.
(2) Klaine, S. J.; Alvarez, P. J. J.; Batley, G. E.; Fernandes, T. F.; Handy, R. D.; Lyon, D. Y.; Mahendra, S.; McLaughlin, M. J.; Lead, J. R. Nanomaterials in the environment: behavior, fate, bioavailability, and effects. *Environ. Toxicol. Chem.* **2008**, *27*, 1825−1851.
(3) Petosa, A. R.; Jaisi, D. P.; Quevedo, I. R.; Elimelech, M.; Tufenkji, N. Aggregation and deposition of engineered nanomaterials in aquatic environments: Role of physicochemical interactions. *Environ. Sci. Technol.* **2010**, *44*, 6532−6549.
(4) Hotze, E. M.; Phenrat, T.; Lowry, G. V. Nanoparticle aggregation: challenges to understanding transport and reactivity in the environment. *J. Environ. Qual.* **2010**, *39*, 1909−1924.
(5) Louie, S. M.; Tilton, R. D.; Lowry, G. V. Critical review: impacts of macromolecular coatings on critical physicochemical processes controlling environmental fate of nanomaterials. *Environ. Sci.: Nano* **2016**, *3*, 283−310.
(6) Gomez-Flores, A.; Bradford, S. A.; Hwang, G.; Heyes, G. W.; Kim, H. Particle−bubble interaction energies for particles with physical and chemical heterogeneities. *Miner. Eng.* **2020**, *155*, 106472.
(7) Gomez-Flores, A.; Bradford, S. A.; Hwang, G.; Choi, S.; Tong, M.; Kim, H. Shape and orientation of bare silica particles influence their deposition under intermediate ionic strength: A Study with QCM−D and DLVO theory. *Colloids Surf., A* **2020**, *599*, 124921.
(8) Gomez-Flores, A.; Bradford, S. A.; Wu, L.; Kim, H. Interaction energies for hollow and solid cylinders: Role of aspect ratio and particle orientation. *Colloids Surf., A* **2019**, *580*, 123781.
(9) Li, T.; Shen, C.; Wu, S.; Jin, C.; Bradford, S. A. Synergies of surface roughness and hydration on colloid detachment in saturated porous media: Column and atomic force microscopy studies. *Water Res.* **2020**, *183*, 116068.
(10) Shen, C.; Bradford, S. A.; Li, T.; Li, B.; Huang, Y. Can nanoscale surface charge heterogeneity really explain colloid detachment from primary minima upon reduction of solution ionic strength? *J. Nanopart. Res.* **2018**, *20*, 165.
(11) Shen, C.; Li, B.; Huang, Y.; Jin, Y. Kinetics of coupled primary- and secondary-minimum deposition of colloids under unfavorable chemical conditions. *Environ. Sci. Technol.* **2007**, *41*, 6976−6982.
(12) Bradford, S. A.; Kim, H.; Shen, C.; Sasidharan, S.; Shang, J. Contributions of nanoscale roughness to anomalous colloid retention and stability behavior. *Langmuir* **2017**, *33*, 10094−10105.
(13) Elimelech, M.; Gregory, J.; Jia, X.; Williams, R. *Particle Deposition and Aggregation Measurement, Modeling and Simulation*. Butterworth-Heinemann: Woburn, MA, 1995; p 448.
(14) Rasmuson, A.; Pazmino, E.; Assemi, S.; Johnson, W. P. Contribution of Nano- to Microscale Roughness to Heterogeneity: Closing the Gap between Unfavorable and Favorable Colloid Attachment Conditions. *Environ. Sci. Technol.* **2017**, *51*, 2151−2160.
(15) Rasmuson, A.; VanNess, K.; Ron, C. A.; Johnson, W. P. Hydrodynamic versus surface interaction impacts of roughness in closing the gap between favorable and unfavorable colloid transport conditions. *Environ. Sci. Technol.* **2019**, *53*, 2450−2459.
(16) Ron, C. A.; VanNess, K.; Rasmuson, A.; Johnson, W. P. How nanoscale surface heterogeneity impacts transport of nano-to microparticles on surfaces under unfavorable attachment conditions. *Environ. Sci.: Nano* **2019**, *6*, 1921−1931.
(17) Shen, C.; Jin, Y.; Zhuang, J.; Li, T.; Xing, B. Role and importance of surface heterogeneities in transport of particles in saturated porous media. *Crit. Rev. Environ. Sci. Technol.* **2020**, *50*, 244−329.
(18) Liang, Y.; Zhou, J.; Dong, Y.; Klumpp, E.; Šimůnek, J.; Bradford, S. A. Evidence for the critical role of nanoscale surface roughness on the retention and release of silver nanoparticles in porous media. *Environ. Pollut.* **2020**, *258*, 113803.
(19) Suresh, L.; Walz, J. Y. Effect of surface roughness on the interaction energy between a colloidal sphere and a flat plate. *J. Colloid Interface Sci.* **1996**, *183*, 199−213.
(20) Bhattacharjee, S.; Elimelech, M.; Borkovec, M. DLVO interaction between colloidal particles: Beyond Derjaguin's approximation. *Croat. Chem. Acta* **1998**, *71*, 883−903.
(21) Hoek, E. M. V.; Bhattacharjee, S.; Elimelech, M. Effect of membrane surface roughness on colloid-membrane DLVO interactions. *Langmuir* **2003**, *19*, 4836−4847.
(22) Hoek, E. M. V.; Agarwal, G. K. Extended DLVO interactions between spherical particles and rough surfaces. *J. Colloid Interface Sci.* **2006**, *298*, 50−58.
(23) Huang, X.; Bhattacharjee, S.; Hoek, E. M. V. Is Surface Roughness a "Scapegoat" or a Primary Factor When Defining Particle−Substrate Interactions? *Langmuir* **20010**, *26*, 2528−2537.
(24) Bendersky, M.; Davis, J. M. DLVO interaction of colloidal particles with topographically and chemically heterogeneous surfaces. *J. Colloid Interface Sci.* **2011**, *353*, 87−97.
(25) Henry, C.; Minier, J.-P.; Lefèvre, G.; Hurisse, O. Numerical study on the deposition rate of hematite particle on polypropylene walls: role of surface roughness. *Langmuir* **2011**, *27*, 4603−4612.
(26) Bradford, S. A.; Torkzaban, S. Colloid interaction energies for physically and chemically heterogeneous porous media. *Langmuir* **2013**, *29*, 3668−3676.
(27) Pazmino, E.; Trauscht, J.; Dame, B.; Johnson, W. P. Power law size-distributed heterogeneity explains colloid retention on soda lime glass in the presence of energy barriers. *Langmuir* **2014**, *30*, 5412−5421.
(28) Shen, C.; Zhang, M.; Zhang, S.; Wang, Z.; Zhang, H.; Li, B.; Huang, Y. Influence of surface heterogeneities on reversibility of fullerene (nC60) nanoparticle attachment in saturated porous media. *J. Hazard. Mater.* **2015**, *290*, 60−68.
(29) Li, T.; Jin, Y.; Huang, Y.; Li, B.; Shen, C. Observed dependence of colloid detachment on the concentration of initially attached colloids and collector surface heterogeneity in porous media. *Environ. Sci. Technol.* **2017**, *51*, 2811−2820.
(30) Bradford, S. A.; Sasidharan, S.; Kim, H.; Hwang, G. Comparison of types and amounts of nanoscale heterogeneity on bacteria retention. *Front. Environ. Sci.* **2018**, *6*, 56.
(31) Wang, H.; Zhang, W.; Zeng, S.; Shen, C.; Jin, C.; Huang, Y. Interactions between nanoparticles and fractal surfaces. *Water Res.* **2019**, *151*, 296−309.
(32) Zhang, M.; Bradford, S. A.; Šimůnek, J.; Vereecken, H.; Klumpp, E. Do goethite surfaces really control the transport and retention of multi-walled carbon nanotubes in chemically heterogeneous porous media? *Environ. Sci. Technol.* **2016**, *50*, 12713−12721.
(33) Bradford, S. A.; Torkzaban, S. Determining parameters and mechanisms of colloid retention and release in porous media. *Langmuir* **2015**, *31*, 12096−12105.
(34) Lin, S.; Wiesner, M. R. Theoretical investigation on the steric interaction in colloidal deposition. *Langmuir* **2012**, *28*, 15233−15245.

(35) Phenrat, T.; Song, J. E.; Cisneros, C. M.; Schoenfelder, D. P.; Tilton, R. D.; Lowry, G. V. Estimating attachment of nano- and submicrometer-particles coated with organic macromolecules in porous media: Development of an empirical model. *Environ. Sci. Technol.* **2010**, *44*, 4531−4538.
(36) Ottofuelling, S.; Von Der Kammer, F.; Hofmann, T. Commercial titanium dioxide nanoparticles in both natural and synthetic water: comprehensive multidimensional testing and prediction of aggregation behavior. *Environ. Sci. Technol.* **2011**, *45*, 10045−10052.
(37) Fleer, G.; Scheujtens, J.; Cohen-Stuart, M.; Vincent, B.; Cosgrove, T. *Polymers at Interfaces*; Chapman Hall: London-Glasgow-New York, 1993.
(38) Lundqvist, M.; Sethson, I.; Jonsson, B.-H. Protein adsorption onto silica nanoparticles: conformational changes depend on the particles' curvature and the protein stability. *Langmuir* **2004**, *20*, 10639−10647.
(39) Roach, P.; Farrar, D.; Perry, C. C. Surface tailoring for controlled protein adsorption: effect of topography at the nanometer scale and chemistry. *J. Am. Chem. Soc.* **2006**, *128*, 3939−3945.
(40) Vertegel, A. A.; Siegel, R. W.; Dordick, J. S. Silica nanoparticle size influences the structure and enzymatic activity of adsorbed lysozyme. *Langmuir* **2004**, *20*, 6800−6807.
(41) Christian, P.; Von der Kammer, F.; Baalousha, M.; Hofmann, T. Nanoparticles: structure, properties, preparation and behaviour in environmental media. *Ecotoxicol* **2008**, *17*, 326−343.
(42) Aiken, G. R.; Hsu-Kim, H.; Ryan, J. N. Influence of dissolved organic matter on the environmental fate of metals, nanoparticles, and colloids. *Environ. Sci. Technol.* **2011**, *45*, 3196−3201.
(43) Ju-Nam, Y.; Lead, J. R. Manufactured nanoparticles: an overview of their chemistry, interactions and potential environmental implications. *Sci. Total Environ.* **2008**, *400*, 396−414.
(44) Pal, N.; Kumar, N.; Mandal, A. Stabilization of dispersed oil droplets in nanoemulsions by synergistic effects of the gemini surfactant, PHPA polymer, and silica nanoparticle. *Langmuir* **2019**, *35*, 2655−2667.
(45) Hwang, G.; Gomez-Flores, A.; Bradford, S. A.; Choi, S.; Jo, E.; Kim, S. B.; Tong, M.; Kim, H. Analysis of stability behavior of carbon black nanoparticles in ecotoxicological media: Hydrophobic and steric effects. *Colloids Surf., A* **2018**, *554*, 306−316.
(46) Yang, W.; Bradford, S. A.; Wang, Y.; Sharma, P.; Shang, J.; Li, B. Transport of biochar colloids in saturated porous media in the presence of humic substances or proteins. *Environ. Pollut.* **2019**, *246*, 855−863.
(47) Adrian, Y. F.; Schneidewind, U.; Bradford, S. A.; Simunek, J.; Fernandez-Steeger, T. M.; Azzam, R. Transport and retention of surfactant- and polymer-stabilized engineered silver nanoparticles in silicate-dominated aquifer material. *Environ. Pollut.* **2018**, *236*, 195−207.
(48) Adrian, Y. F.; Schneidewind, U.; Bradford, S. A.; Šimůnek, J.; Klumpp, E.; Azzam, R. Transport and retention of engineered silver nanoparticles in carbonate-rich sediments in the presence and absence of soil organic matter. *Environ. Pollut.* **2019**, *255*, 113124.
(49) Wilkinson, K. J.; Balnois, E.; Leppard, G. G.; Buffle, J. Characteristic features of the major components of freshwater colloidal organic matter revealed by transmission electron and atomic force microscopy. *Colloids Surf., A* **1999**, *155*, 287−310.
(50) Meinders, J. M.; van der Mei, H. C.; Busscher, H. J. Physicochemical Aspects of Deposition of Streptococcus thermophilus B to Hydrophobic and Hydrophilic Substrata in a Parallel Plate Flow Chamber. *J. Colloid Interface Sci.* **1994**, *164*, 355−363.
(51) Meinders, J. M.; van der Mei, H. C.; Busscher, H. J. Deposition efficiency and reversibility of bacterial adhesion under flow. *J. Colloid Interface Sci.* **1995**, *176*, 329−341.
(52) Stuart, J. K.; Hlady, V. Effects of discrete protein-surface interactions in scanning force microscopy adhesion force measurements. *Langmuir* **1995**, *11*, 1368−1374.
(53) Hemmerle, J.; Altmann, S. M.; Maaloum, M.; Horber, J. K. H.; Heinrich, L.; Voegel, J. C.; Schaaf, P. Direct observation of the anchoring process during the adsorption of fibrinogen on a solid surface by force-spectroscopy mode atomic force microscopy. *Proc. Natl. Acad. Sci. U.S.A.* **1999**, *96*, 6705−6710.
(54) Mondon, M.; Berger, S.; Ziegler, C. Scanning-force techniques to monitor time-dependent changes in topography and adhesion force of proteins on surfaces. *Anal. Bioanal. Chem.* **2003**, *375*, 849−855.
(55) Vadillo-Rodríguez, V.; Busscher, H. J.; Norde, W.; de Vries, J.; van der Mei, H. C. Atomic force microscopic corroboration of bond aging for adhesion of Streptococcus thermophilus to solid substrata. *J. Colloid Interface Sci.* **2004**, *278*, 251−254.
(56) Xu, L.-C.; Logan, B. E. Adhesion forces between functionalized latex microspheres and protein-coated surfaces evaluated using colloid probe atomic force microscopy. *Colloids Surf., B* **2006**, *48*, 84−94.
(57) Xu, L.-C.; Vadillo-Rodriguez, V.; Logan, B. E. Residence time, loading force, pH, and ionic strength affect adhesion forces between colloids and biopolymer-coated surfaces. *Langmuir* **2005**, *21*, 7491−7500.
(58) Torkzaban, S.; Bradford, S. A.; Wan, J.; Tokunaga, T.; Masoudih, A. Release of quantum dot nanoparticles in porous media: role of cation exchange and aging time. *Environ. Sci. Technol.* **2013**, *47*, 11528−11536.
(59) Fang, B.; Jiang, Y.; Rotello, V. M.; Nüsslein, K.; Santore, M. M. Easy come easy go: surfaces containing immobilized nanoparticles or isolated polycation chains facilitate removal of captured Staphylococcus aureus by retarding bacterial bond maturation. *ACS Nano* **2014**, *8*, 1180−1190.
(60) Sasidharan, S.; Bradford, S. A.; Torkzaban, S.; Ye, X.; Vanderzalm, J.; Du, X.; Page, D. Unraveling the complexities of the velocity dependency of E. coli retention and release parameters in saturated porous media. *Sci. Total Environ.* **2017**, *603−604*, 406−415.
(61) Torkzaban, S.; Bradford, S. A. Critical role of surface roughness on colloid retention and release in porous media. *Water Res.* **2016**, *88*, 274−284.
(62) Hogg, R.; Healy, T. W.; Fuerstenau, D. W. Mutual coagulation of colloidal dispersions. *Trans. Faraday Soc.* **1966**, *62*, 1638.
(63) Torkzaban, S.; Tazehkand, S. S.; Walker, S. L.; Bradford, S. A. Transport and fate of bacteria in porous media: Coupled effects of chemical conditions and pore space geometry. *Water Resour. Res.* **2008**, *44*, W04403.
(64) Gregory, J. Approximate expressions for retarded van der waals interaction. *J. Colloid Interface Sci.* **1981**, *83*, 138−145.
(65) Rijnaarts, H. H. M.; Norde, W.; Bouwer, E. J.; Lyklema, J.; Zehnder, A. J. B. Reversibility and mechanism of bacterial adhesion. *Colloids Surf., B* **1995**, *4*, 5−22.
(66) Rijnaarts, H. H. M.; Norde, W.; Lyklema, J.; Zehnder, A. J. B. The isoelectric point of bacteria as an indicator for the presence of cell surface polymers that inhibit adhesion. *Colloids Surf., B* **1995**, *4*, 191−197.
(67) Oliveira, R. Understanding adhesion: A means for preventing fouling. *Exp. Therm. Fluid Sci.* **1997**, *14*, 316−322.
(68) Van Oss, C. *Interfacial Forces in Aqueous Media*; Taylor & Francis Group: New York, 1994; Vol. *1*, pp 18−46.
(69) Alexander, S. Adsorption of chain molecules with a polar head a scaling description. *J. Phys.* **1977**, *38*, 983−987.
(70) de Gennes, P. Dry spreading of a liquid on a random surface. *C. R. Seances Acad. Sci. Ser. 2 Mec. Phys. Chim. Sci. Univers Sci. Terre* **1985**, *300*, 129−132.
(71) Byrd, T. L.; Walz, J. Y. Interaction force profiles between Cryptosporidium parvum oocysts and silica surfaces. *Environ. Sci. Technol.* **2005**, *39*, 9574−9582.
(72) Suresh, L.; Walz, J. Y. Direct measurement of the effect of surface roughness on the colloidal forces between a particle and flat plate. *J. Colloid Interface Sci.* **1997**, *196*, 177−190.
(73) Bradford, S. A.; Leij, F. J.; Schijven, J.; Torkzaban, S. Critical role of preferential flow in field-scale pathogen transport and retention. *Vadose Zone J.* **2017**, *16*, 1.


https://dx.doi.org/10.1021/acs.langmuir.0c03029
*Langmuir* 2021, 37, 1501−1510